THE MECHANISM OF BINDING BETWEEN THE *PLASMODIUM FALCIPARUM* H-PROTEIN AND LIPOATE LIGASE 1

by
Ryan E. Rodriguez

A thesis submitted to Johns Hopkins University in conformity with the requirements for the degree of Master of Science

Baltimore, Maryland
April, 2015

Abstract

Malaria is a devastating tropical disease, accounting for 2 million infections and 440,000 deaths in 2015. The most effective treatment for malaria is chemotherapy to kill the blood stage parasite. Recent spread of drug resistance against the most effective anti-malarial known, raises concerns about the future efficacy of existing blood stage chemotherapy.

It is therefore necessary to identify and study unique biochemical pathways in the parasite that hold the potential for chemical intervention. Mitochondrial lipoylation in *Plasmodium falciparum* is one such pathway. Recent evidence suggests that mitochondrial lipoylation in the blood stage uses a novel redox mechanism. This pathway appears to be a suitable drug target for blood stage malaria and further characterization of the mechanisms involved are needed.

In this study two of the key proteins involved in this pathway, lipoate ligase 1 (LipL1) and the H-protein, were expressed in *E. coli* and purified using FPLC. The purified proteins along with the cofactors necessary to drive the protein-protein interaction were screened for crystal formation in an attempt to collect x-ray diffraction data that could be used for structural determination. Crystals were grown and subjected to x-ray radiation, but produced poor quality diffraction data and no structural determinations could be made.

The dissociation constant and binding kinetics of the protein-protein interaction under reducing and non-reducing conditions were studied using isothermal titration calorimetry (ITC). Data collected from ITC experiments yielded an average dissociation

constant of 0.097µM under non-reducing conditions and 4.8µM under reducing conditions. Surface Plasmon Resonance (SPR), which uses a fraction of the protein sample compared to ITC, was also used to study the binding between LipL1 and the H-protein. Data collected from SPR experiments yielded a dissociation constant of 0.39µM under non-reducing conditions.

The above dissociation constants suggest that lipoylation of the H-protein takes place due to its increased affinity for the LipL1-lipoyl-AMP complex, which dominates under non-reducing conditions. Under very reducing conditions, the LipL1-dihydrolipoyl-AMP complex dominates and as can be inferred from the dissociation constants, binding and subsequent lipoylation of the H-protein is diminished allowing for binding or lipoylation of other substrates.

Thesis Readers

Dr. Sean Prigge, Department of Molecular Microbiology and Immunology

Dr. Jürgen Bosch, Department of Biochemistry and Molecular Biology

Acknowledgements

First, I would like to thank my beautiful wife Nathalie for her continued support and dedication to our growing family. I have no idea where or what I would be without her by my side. My wonderful mother, Wanda, for her continued encouragement and unconditional love.

Dr. Sean Prigge for his guidance, his patience and for allowing me to stumble through the research process in his lab. The Prigge lab members that I have worked and become acquainted with over the past two years – Aleah, Alfredo, Hugo and Russel – thanks for answering all of my questions and pointing me in the right direction. Dr. Jürgen Bosch for his assistance, knowledge, and his time in answering all things SPR related. A huge thank you to Dr. Siva Mandjiny, Dr. Paul Flowers, and Dr. Harold Teague for believing in and supporting me as a young undergraduate student.

Lastly, thank you to the United States Army and the United States Military Academy at West Point for granting me this opportunity to broaden my knowledge base and continue my professional development as a Commissioned Officer.

Table of Contents

Abstract ii

Acknowledgments iv

Table of Contents v

List of Tables vii

List of Figures viii

Introduction

Malaria 1

Malaria Lifecycle 1

Drug Resistance in Malaria 4

Alpha Lipoic Acid 6

Synthesis and Scavenging of Lipoate 6

Lipoate's Dual Role 8

Lipoylation Pathways in *P. falciparum* 10

Structural Studies of *E. coli* lipoylation 12

Aims of the Project 13

Materials and Methods

Expression Plasmids 14

Protein expression and purification 17

Crystallization 19

Isothermal Titration Calorimetry 20

Surface Plasmon Resonance 20

Results

Protein purification 23

Crystallization 25

Isothermal Titration Calorimetry 26

Surface Plasmon Resonance 28

Discussion 30

Appendix 35

References 44

List of Tables

Table 1. α-KDH complex substrates 9

Table 2. Crystal tray optimization conditions #1 37

Table 3. Crystal tray optimization conditions #2 38

Table 4. Crystal tray optimization conditions #3 39

Table 5. Crystal tray optimization conditions #4 40

Table 6. Crystal tray optimization conditions #5 41

Table 7. SPR experimental notes 42

Table 8. ITC results 43

List of Figures

Figure 1. Lifecycle of the human malaria parasite 3

Figure 2. Octanoic acid derivatives 6

Figure 3. Reactions of lipoylated complexes 10

Figure 4. Lipoylation via lipoate scavenging in *P. falciparum* 12

Figure 5. HK96A and LipL1 protein purification 24

Figure 6. Fusion protein purification 25

Figure 7. LipL1-HK96A protein complex crystals 26

Figure 8. ITC binding data – non-reducing conditions 27

Figure 9. ITC binding data – reducing conditions 28

Figure 10. SPR binding data – non-reducing conditions 30

Figure 11. HK96M-LipL1 DNA sequence 36

Figure 12. HK96M-LipL1 amino acid sequence 36

Introduction

Malaria

There have been great strides made in the reduction of malaria cases and deaths over the past 15 years. This reduction is due to a number of factors such as increased distribution and use of insecticide-treated mosquito nets (ITNs), increased coverage of indoor residual spraying (IRS), increased chemoprevention in pregnant women and children, increased distribution and use of diagnostic testing, specifically rapid diagnostic tests (RDTs), and increased use of artemisinin-based combination therapy (ACT) as antimalarial drug treatment (1). Although there have been great reductions in the number of malaria cases and deaths over the past 15 years, malaria remains a devastating disease. The World Health Organization (WHO) estimates that there were 214 million malaria cases and 440,000 malaria related deaths in 2015 and nearly 70% (306,000) of those deaths occurred in children under the age of 5 (1).

Malaria Lifecycle

Malaria is a disease caused by the intracellular, protozoan parasites of the genus *Plasmodium*. Humans can become infected with the *Plasmodium* parasite when they are bitten by an infectious female *Anopheles* mosquito. Currently, five species of *Plasmodium*: *P. falciparum, P. knowlesii, P. malariae, P. ovale and P. vivax* are known to cause disease in humans. Of the five species of *Plasmodium* that infect humans, *P. falciparum* accounts for the majority of malaria related deaths (1).

To say that the lifecycle of the *Plasmodium* parasite is complex is an

understatement. Upon probing for a blood meal, the infectious female *Anopheles* mosquito releases the sporozoite form of the parasite from her salivary gland into the human host via her proboscis (figure 1). Sporozoites migrate through the human bloodstream into the liver where they invade hepatocytes. Once in the hepatocyte, the sporozoite undergoes replication for 2-16 (species dependent (sd)) days until thousands of merozoites are released into the blood stream. These merozoites invade erythrocytes, where they undergo schizogony to produce 8-32 (sd) new merozoites per infected erythrocyte. The infected erythrocyte ruptures 48-72 (sd) hours' post-invasion releasing merozoites which invade more erythrocytes and perpetuate the asexual erythrocytic or blood stage cycle (2). A subset of merozoites differentiate into male and female gametocytes within the erythrocyte. These non-replicating, asymptomatic gametocytes are responsible for parasite transmission back into the mosquito vector upon ingestion of a blood meal. Once inside the mosquito midgut, the gametocytes differentiate into male and female gametes and fuse to form a zygote. The zygote further develops into another form of the parasite known as an ookinete. Once formed, the ookinete moves through the mosquito mid-gut epithelium and forms an oocyst on the outer midgut epithelium. Thousands of sporozoites are produced in each oocyst and after rupture of the oocyst they migrate to the mosquito salivary gland where they wait to be transmitted to the human host during the next blood meal (2).

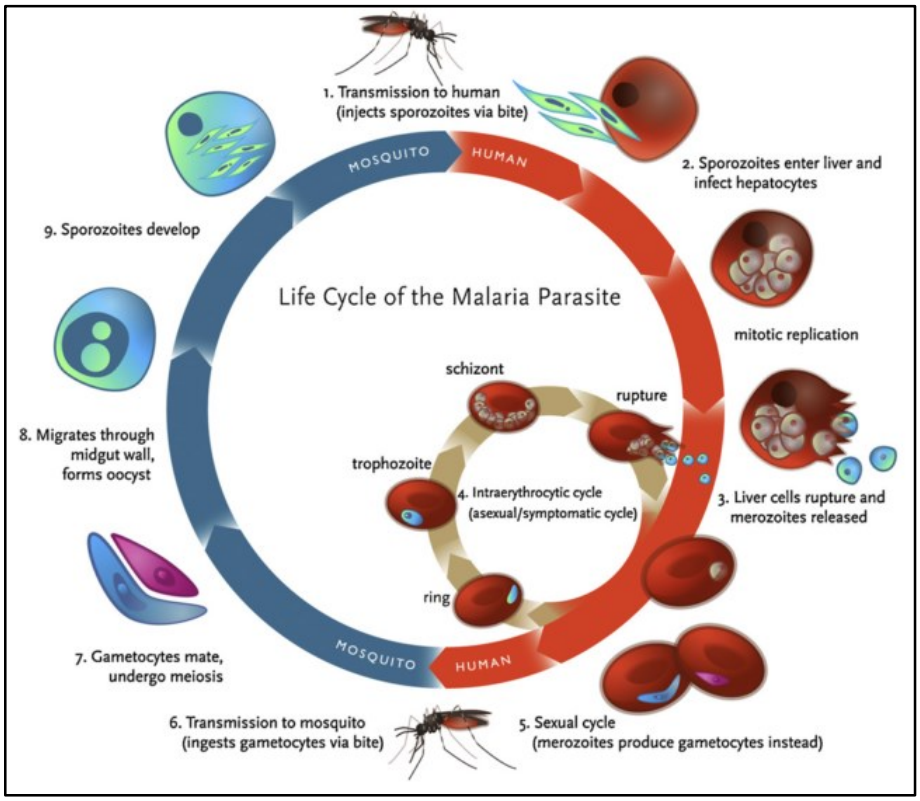

Figure 1. Lifecycle of the human malaria parasite (2).

This complicated two organism life cycle offers many hurdles in the pursuit to control malaria, however, an optimist would contest that it also offers many opportunities to disrupt the parasite at various stages during its lifecycle. There are numerous labs dedicated to understanding the interplay of the parasite and its host environment in all stages of the lifecycle. The research in the laboratory of Dr. Sean Prigge is primarily dedicated to studying the blood stage of *P. falciparum*, since this is the only stage that causes the clinical symptoms of malaria in people. The work presented in this thesis is concentrates on the mechanism of protein lipoylation in the mitochondrion – a process known to be essential for the survival of blood stage *P. falciparum* parasites.

Drug Resistance in Malaria

One of the remaining challenges for malaria control and elimination is the geographical spread of drug resistant parasites (1). Drugs have been used to prevent and treat persons infected with malaria for centuries. Chloroquine (CQ), an antimalarial first synthesized in the 1930's, became widely used in the early 1950's due its safety, low cost, and efficacy. CQ resistant parasites were anecdotally reported in 1957 and in 1960 the first CQ resistant parasites were confirmed in Colombia and also along the Cambodia-Thailand border. Over the next three decades CQ resistant parasites spread from the Cambodia-Thai border throughout Southeast Asia, Micronesia, Melanesia, India, and into Africa. By 1987 CQ resistant parasites had been confirmed in more than 40 countries. The emergence of CQ resistant parasites reduced the therapeutic efficacy of CQ as an antimalarial in these regions, but also severely hampered early malaria eradication efforts (2–4).

Sulfadoxine-pyrimethamine (SP), a safe and cheap antimalarial treatment, began seeing widespread use as CQ resistant parasites began to spread. Sulfadoxine and pyrimethamine target and inhibit two enzymes involved in folate metabolism, a different mechanism of action than CQ (5). SP was introduced in Thailand in the late 1960's and its use spread throughout Southeast Asia and South America in the 1970's and eventually saw use in Africa in the early 1980's (6–9). Just as was seen with CQ, increased use of SP led to increased parasite resistance; in the 1980's SP failure rates were between 60-70% in parts of Thailand, in the 1990's many endemic regions of South America could no longer effectively use SP treatment, and in Africa SP resistance was

first documented in the 1980's and rapidly spread from East Africa into West Africa (7–11).

Artemisinin was first reported to cure malarious patients in China in 1979 (12). It was first introduced on the world stage in the mid 1990's as multidrug resistant parasites had developed in Southeast Asia. Artemisinin and its derivatives clear blood stage parasites more rapidly than any other currently available antimalarials and artemisinin in combination with other antimalarial drugs (called ACT) has been recommended by the WHO as a treatment for drug resistant *P. falciparum* malaria since 2001 (13, 14). The WHO has also strongly recommended that artemisinin only be used in combination with other antimalarials and in 2006 urged artemisinin manufacturers to stop marketing artemisinin monotherapies; both of these recommendations were made to help combat the possibility of artemisinin resistant parasites (4, 14). Despite the WHOs best efforts, ACT resistant parasites have recently emerged in Southeast Asia (13, 15, 16).

The possibility of ACT resistant parasite spreading into other parts of the world poses a major threat to global malaria control efforts, as ACT is one of the last remaining treatments for multi drug resistant *P. falciparum* malaria. In an effort to combat the spread of malaria, it is necessary to find novel or existing compounds that lack adverse effects in the human host, but are effective at clearing parasites during blood stage infection. One approach to uncovering these compounds is the biochemical and structural characterization of pathways that are unique to the parasite. One particular pathway of interest as a target for drug intervention is the mitochondrial lipoylation

pathway in *P. falciparum.*

Alpha Lipoic Acid

α-lipoic acid is an eight carbon cyclic disulfide derivative of octanoic acid (figure 2). Above pH 4.7 the deprotonated and charged form, lipoate, exists as the dominate species (17). α-lipoic acid was first crystallized from liver extracts in 1951 and at the time was thought to be a novel B vitamin due to its ubiquity in biological sources, high activity, and evidence of its catalytic role in the oxidative decarboxylation of pyruvate (17). The notion of lipoate as a B vitamin has since been abandoned as there is no known human disease associated with lipoate deficiency and strong evidence exists for mammalian synthesis of lipoate (18). Nevertheless, lipoate plays a key role as a cofactor in several metabolic pathways.

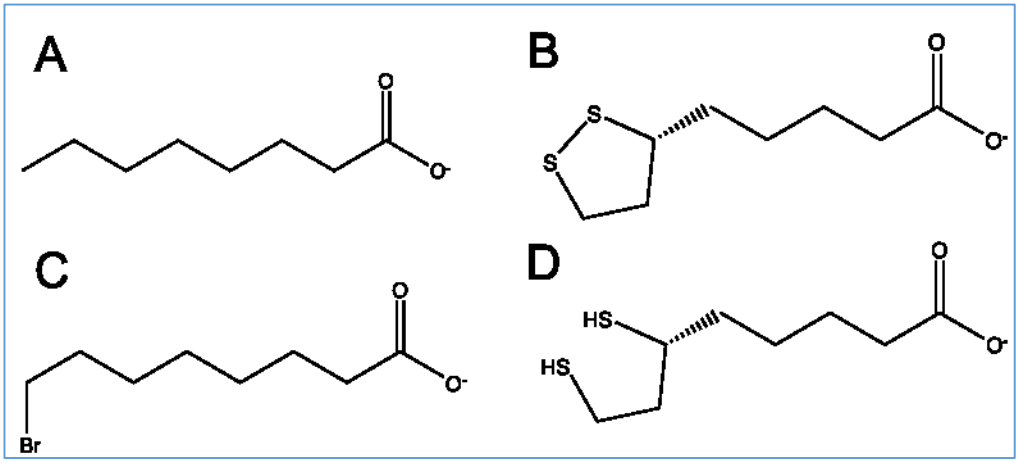

Figure 2. Octanoic acid derivatives. (A) Octanoic acid in its deprotonated form. (B) The R stereoisomer of lipoate. (C) The structural analogue 8-bromooctanoate has been used in parasite growth inhibition studies. (D) The reduced form of lipoate, dihydrolipoate.

Synthesis and Scavenging of Lipoate

Lipoylation is the term used to describe the posttranslational modification or covalent attachment of lipoate to proteins. Two mechanisms of lipoylation are known to

exist: lipoate scavenging, which refers to the ligation of free exogenous lipoate to a protein and lipoate synthesis, which refers to the generation of protein bound lipoate from an 8-carbon, octanoylated precursor (19).

Lipoate metabolism is present in most bacterial, fungal, and protozoan pathogens and a thorough review of the nuances of the lipoylation strategies and lipoylated proteins present in these pathogens can be found in reference (20). The two mechanisms of lipoylation have been best characterized in *E. coli* and will be described here, before introducing the pathways in *Plasmodium*.

In *E. coli*, lipoate scavenging occurs through the ligation of free exogenous lipoate by a lipoate ligase, LplA, to a conserved lysine residue on either of the apo-E2 or apo-H-protein subunits of the known lipoylated complexes (described below) (21). All lipoate ligases work in similar manner to catalyze a two-step ATP dependent reaction: 1. ATP activates free lipoate to form lipoyl-AMP, releasing pyrophosphate. 2. Upon binding of apo-E2 or apo-H-protein subunits, the activated carbonyl of lipoyl-AMP forms a lipoamide bond with a conserved terminal lysine residue on these proteins, releasing AMP and the now lipoylated holo-E2 or holo-H-proteins (21). It has also been shown that LplA can use octanoate and 8-bromooctanoate as a substrate in lieu of lipoate, with 8-bromooctanoate resulting in *E. coli* growth inhibition (21–23).

Lipoate synthesis in *E. coli* is catalyzed by an octanoyl transferase, LipB, which transfers an octanoyl group from octanoyl acyl carrier protein to the apoproteins, E2 or H (19). After this transfer, a lipoate synthase, LipA, inserts two sulfur atoms on the octanoylated proteins forming the dithiolane ring of lipoate (19, 22, 24).

It is worth noting that the lipoyl domain of the E2 subunits and the H-protein share structural similarities, as would be expected considering that they are modified by the same lipoylation enzymes (27).

Lipoate's Dual Role

Lipoate plays two major roles in the cell. First, lipoate is a unique antioxidant as it confers free radical protection in both its oxidized and reduced forms. The lipoate – dihydrolipoate redox couple and its wide ranging antioxidant properties can be reviewed in references (25) and (26). Second, lipoate serves as a key co-factor in several multi-enzyme complexes involved in metabolism. Three of these five complexes are α-ketoacid dehydrogenases, the fourth is an acetoin dehydrogenase, and the fifth is the glycine cleavage complex (GCV) or glycine cleavage system (GCS) (20).

The three α-ketoacid dehydrogenase complexes are pyruvate dehydrogenase (PDH), α-ketoglutarate dehydrogenase (KDH), and branched-chain α-ketoacid dehydrogenase (BCDH). These three α-ketoacid dehydrogenase complexes as well as the acetoin dehydrogenase complex share a three subunit architecture with the three subunits commonly referred to as E1, E2, and E3 (27, 28). These dehydrogenase complexes are massive; the bovine heart PDH complex, for example, is 9.5 MDa and consists of 30 copies of the E1 heterotetramer, 12 copies of the E3-binding protein monomer, and 12 copies of the E3 homodimer all arranged around a 20 copy core of the E2 trimer in an icosahedral configuration (29). The GCS has a much different architecture as no stable complex is formed, it is composed of four loosely associated

and independent proteins, known as P, T, H and L (30).

The α-ketoacid dehydrogenase complexes all work in a similar manner in that they catalyze the decarboxylation of α-ketoacids to produce acyl-coenzyme A (acyl-CoA), NADH, and CO_2 by related reaction mechanisms (27). Essentially, the reactions begin with the decarboxylation of the substrate by the E1 subunit and acylation of one of the sulfur atoms in lipoamide, leaving the second sulfur reduced. The E2 subunit active site catalyzes the transfer of the acyl moiety from the lipoamide to CoA. The E3 subunit then oxidizes the reduced dihydrolipoamide back to lipoamide in a NAD-dependent reaction (27) (figure 3A). The various substrates and fates of the α-ketoacid complexes can be in found in table 1.

α-ketoacid complex	**Substrate**	**Products**	**Pathways**
PDH	pyruvate	Acetyl-CoA	TCA cycle Fatty acid synthesis Fatty acid elongation Isoprenoid biosynthesis
KDH	α-ketoglutarate	Succinyl-CoA	TCA cycle Heme biosynthesis Amino acid biosynthesis
BCDH	α-ketoisovalerate α-ketoisocaproate α-keto-β-methylvalerate	Isobutyryl-CoA Isovaleryl-CoA α-methylbutyryl-CoA	TCA cycle intermediates Branched chain fatty-acid biosynthesis

Table 1. α-KDH complex substrates. The various substrates of the α-KDH complexes, the products that are produced and the relevant metabolic pathways.

The glycine cleavage complex catalyzes the reversible decarboxylation of glycine into CO_2, NADH, NH_3, while transferring a methylene group to tetrahydrofolate (THF) forming 5,10-CH_2-THF (30). 5,10-CH_2-THF then serves as a one-carbon donor molecule,

used by the cell primarily during the synthesis of pyrimidine nucleotides (31) (figure 3B).

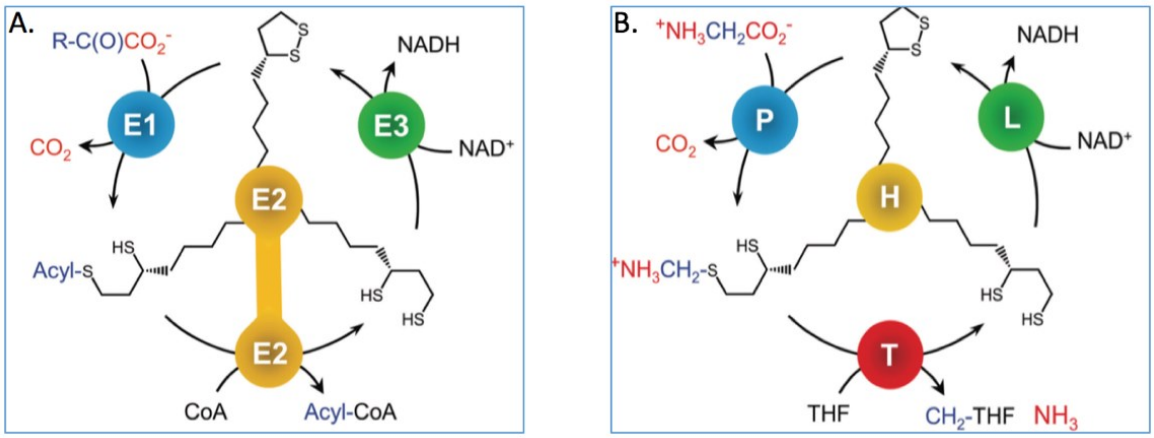

Figure 3. Reactions of lipoylated complexes (20)*. (A) The α-Ketoacid dehydrogenase complexes have analogous reaction mechanisms. The E1 subunit decarboxylates the substrate and transfers the acyl group to lipoamide on the E2 subunit. The E2 subunit transfers the acyl group to coenzyme A. Lipoate is regenerated through reduction of NAD+ by the E3 subunit. (B) The Glycine cleavage complex catalyzes the reversible oxidative decarboxylation of glycine into carbon dioxide, ammonia, and a methylene group. The H-protein serves as a mobile substrate, shuttling between the active sites of the P, T and L proteins.*

Lipoylation pathways in *P. falciparum*

The *P. falciparum* genome encodes four proteins that are expressed and lipoylated in blood stage parasites, the E2 subunits of the PDH, KDH, BCDH and the H-protein (32–34). The E2 proteins of the KDH and BCDH contain a single lipoyl domain while the PDH E2 contains two lipoyl domains (35). The lipoylated proteins are partitioned in two different organelles within the parasite, the apicoplast and mitochondrion (36).

The apicoplast harbors a lipoate biosynthesis pathway that has been shown to be superfluous during blood stage infection, but critical for parasite development during the liver stage (34, 37, 38). The PDH complex is localized solely to the parasite apicoplast and the lipoylation of the PDH E2 subunit proceeds in a manner analogous to

E. coli lipoate synthesis, with *Pf*LipB acting as the octanoyl transferase and *Pf*LipA serving as the lipoate synthase (35, 36). The *P. falciparum* LipB gene has been successfully disrupted with no deleterious growth defects on blood stage parasites, suggesting that the *P. falciparum* lipoate synthesis pathway is dispensable during the blood stage and therefore would not make a suitable drug target.

The parasite is dependent upon host scavenged lipoate in order to lipoylate the E2 subunits of the BCDH and KDH as well as the H-protein of the GCS, all three of which are found exclusively in the mitochondrion (33, 36, 39). Substrate lipoylation in the parasite mitochondrion is dependent upon two enzymes, lipoate ligase 1 (LipL1) and lipoate ligase 2 (LipL2). LipL1 is strictly localized to the mitochondrion, while LipL2 is found in both the mitochondrion and the apicoplast (34, 36). Both LipL1 and LipL2 genes appear to be refractory to disruption, suggesting that the lipoate scavenging pathway is necessary for parasite blood stage development and therefore would make an attractive target for therapeutic intervention (40, 41). The evidence for the necessity of lipoate scavenging is further strengthened by inhibition studies conducted with the lipoate analogue 8-bromooctanoate (8-BrO) (figure 2). Treatment of parasites with 8-BrO, which is presumed to enter the parasite via the same transporter as lipoate, interferes with the integration of scavenged lipoate and results in blood stage growth inhibition (33).

A recently published paper from our lab provides evidence for two distinct mitochondrial lipoylation pathways in *P. falciparum*. The findings also suggest that the switch between these pathways is dependent upon the redox conditions within the

mitochondrion, a mechanism that has not been described in any other organism (42). Under slightly reducing conditions LipL1 works independently to lipoylate the H-protein. However, under strong reducing conditions LipL1 and LipL2 work in conjunction to almost exclusively lipoylate the E2 subunits of the BCDH and KDH complexes, while the H-protein shows almost no lipoylation as visualized by western blot analysis in (42). The current model for *P. falciparum* mitochondrial lipoylation can be seen in figure 4.

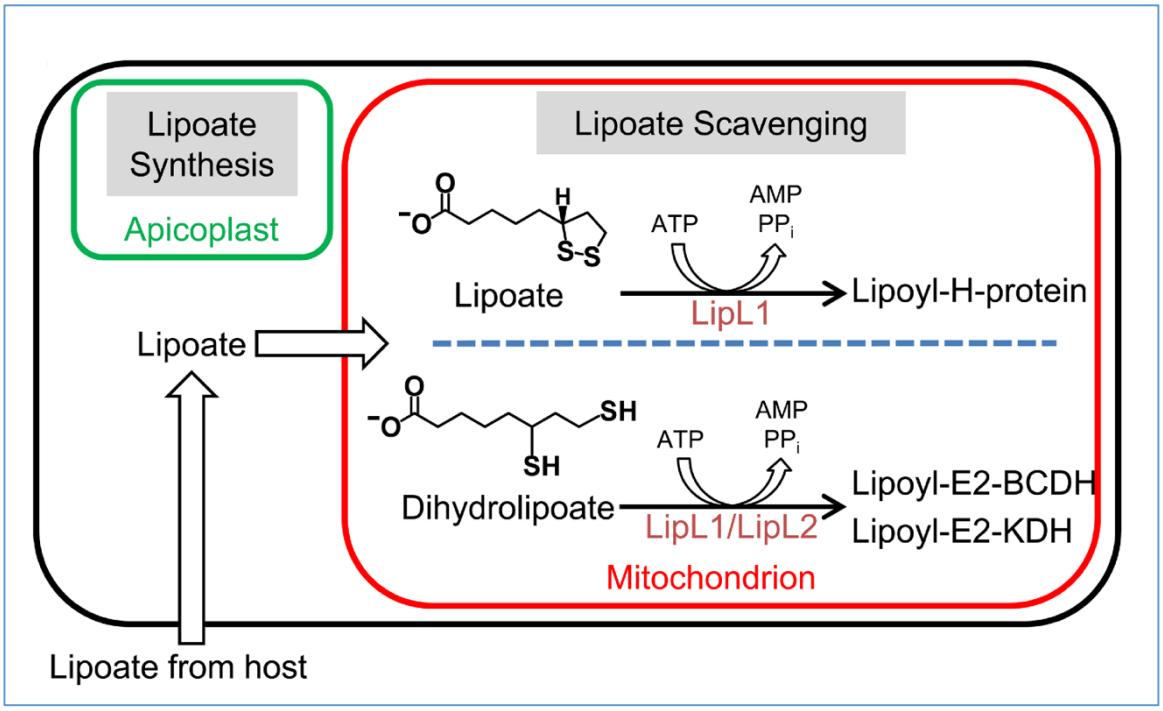

Figure 4 – Lipoylation via lipoate scavenging in P. falciparum. Under less reducing conditions LipL1 lipoylates the H-protein. Under conditions where lipoate is reduced to dihydrolipoate LipL1 and LipL2 work in concert to lipoylate the E2 subunits of the BCDH and KDH complexes.

Structural studies of *E. Coli* lipoylation

A key to understanding what may be going on in the *P. falciparum* mitochondrion can be found if we turn our attention back to the *E. coli* lipoylation

machinery. The crystal structure of the *E. Coli* lipoate ligase, LplA, in complex with lipoyl-AMP has been determined at 2.05 Å as well as the ternary structure of LplA, octanyl-AMP, and the *E. coli* H-protein at 3.00 Å (43). Their structures show that upon activation of lipoate to lipoyl-AMP, LplA undergoes a structural rearrangement where the C-terminal domain rotates by 180^{o}. It is only after this structural rearrangement that binding and subsequent lipoylation of the H-protein can occur.

Aims of the project.

I hypothesize based on evidence from the Afanador (42) paper that *Pf*LipL1 undergoes different structural rearrangements depending on whether it binds lipoyl-AMP or the reduced dihydrolipoyl-AMP. This structural difference is the molecular switch causing LipL1 to recruit either LipL2 (for the lipoylation of KDH and BCDH), or the H-protein. I would therefore predict that the H-protein would bind tightly to a LipL1/ lipoyl-AMP complex, but not to a LipL1/ dihyrolipoyl-AMP complex. Unfortunately, formation of the ternary H-protein/LipL1/lipoyl-AMP complex should rapidly lead to product formation. By mutating the site of lipoylation on the H-protein, from lysine to alanine (HK96A), we can theoretically abrogate its lipoylation while still being able to study the binding.

Using the HK96A mutant, I attempted to crystallize the H-protein/LipL1/lipoyl-AMP complex in order to determine its structure using x-ray crystallography. I also set out to determine the dissociation constant of HK96A for the LipL1/lipoyl-AMP complex under reducing and non-reducing conditions using isothermal titration calorimetry and surface plasmon resonance. The work is done in an attempt to better characterize and

understand the mechanisms of mitochondrial lipoylation in *Plasmodium falciparum*, as this pathway is unique to the parasite and appears to be a good target for drug development against blood stage malaria.

Materials and Methods

Expression Plasmids

Expression plasmid pMALcHT-Hprot (42), encoding residues E35-K200 (lacking the predicted N-terminal mitochondrial transit peptide) of the *Pf* H-protein (PF3D7_1132900) was subjected to site directed mutagenesis (SDM) in order to mutate the conserved lysine residue at position 96 to an alanine residue for binding studies. pMALcHT-Hprot was subjected to PCR amplification with forward and reverse primers coding for the lysine to alanine mutation (see appendix - primers). The resulting PCR reaction mixture was incubated with DpnI endonuclease at 37^{o}C for 1hour to digest any of the template pMALcHT-Hprot plasmid. The amplicons were then subjected to ethanol precipitation and re-suspended in H_2O. Plasmids were transformed into BL21-Star (DE3) cells (Invitrogen), grown for 1 hour in SOC media at 37^{0}C, 250rpm and plated on LB agar + carbenicillin to select for the pMALcHT plasmid. After 24 hours at 37^{o}C colonies were selected, grown in 5ml of circle grow media + carbenicillin overnight at 37^{0}C, 250rpm. Plasmids were isolated using Qiagen plasmid mini-prep protocol and sent for DNA sequencing for verification. One of the three colonies sent for sequencing was verified as having the lysine to alanine mutation at position 96. This plasmid was renamed

pMALcHT-HK96A for this study. Expression plasmid pMALcHT-LipL1 (42) was used without modification for this study.

A plasmid encoding the *Pf* H-protein (residues E35-K200) with a lysine to methionine mutation at position 96 (HK96M) fused to *Pf* LipL1 (minus the mitochondrial targeting sequence) via a 17 amino acid linker region was purchased from GeneArt (appendix, figures 12, 13). This fusion protein construct was designed to be used for crystallization studies and was named pMK HK96M-LipL1 for this study. We used pMK HK96M-LipL1 to generate a similar plasmid with the K96A mutation instead of K96M. pMK HK96M-LipL1 was incubated with restriction enzymes PvuI-HF and AatII overnight at 37^{o}C to remove a small sequence including the lysine to methionine mutation at position 96. One hour prior to gel purification of the cut plasmid, 0.5µl of Shrimp Alkaline Phosphatase (NEB) was added to the reaction to remove the 5' and 3' terminal phosphates. The cut pMK plasmid was visualized on a 1% agarose gel and the resulting band was excised and gel purified using a Qiagen QIAquick gel extraction kit. Duplex DNA encoding the K96A mutation was formed from adaptamer primers (see appendix). 1µL of 100µM forward and reverse HK96A adaptamer primers were mixed with 1µL of 10x PCR buffer (NEB) and 8µL of water. This mixture was placed in a heat block at 92^{o}C for one minute and allowed to cool/anneal at room temperature. After cooling, the duplex DNA insert was diluted to a concentration of 1µM and 0.1µM. A 12µL ligation reaction was initiated using 6µL of New England Biolabs (NEB) 2x ligase buffer, 1.2µL quick ligase (NEB), and 4.8µL of the cut pMK plasmid. After mixing, this 12µL reaction was immediately split into 3 equal parts and incubated with 2µL H_20 (control), 2µL of

1µM HK96A adaptamer, and 2µL of 0.1µM HK96A adaptamer. After 15 minutes at room temperature, these ligation reactions were transformed into Top10 *E. coli* cells (Invitrogen) as described above. Plasmids from carbenicillin-resistant colonies were isolated and sequence verified as described above. The resulting plasmid was named pMK HK96A-LipL1.

The protein coding portions of the pMK plasmids were subcloned into the expression plasmid pMALcHT (44) for protein production. pMK HK96M-LipL1 and pMK HK96A-LipL1 were digested with EcoRI and HindIII overnight at 37^{o}C to remove the H-LipL1 fusion sequence from the plasmid. The digestion products were visualized on a 1% agarose gel and the band corresponding to the H-LipL1 sequence was excised and gel purified as described above. This sequence was then ligated into the pMALcHT vector which had also been digested with EcoRI and HindIII. The sequences were verified and the resulting plasmids were renamed pMALcHT HK96M-LipL1 and pMALcHT HK96A-LipL1.

The HK96A-LipL1 fusion construct was designed with multiple restriction enzyme sites in the 17 amino acid linker region between the two proteins in order to have the option to adjust the length of the linker (appendix, figure 12). The restriction enzymes SpeI and NheI were used to cut out a 15 amino acid stretch of this linker. The cut plasmid was visualized on a 1% agarose gel, the band was cut out, gel purified, and subjected to ligation. The sequence was verified and the product was renamed pMALcHT HK96A-LipL1 d15. Another truncation was made in a similar manner with the

restriction enzyme KpnI-HF, removing 9 amino acids from the linker region. The sequence of this construct was verified and was renamed pMALcHT HK96A-LipL1 d9.

Expression plasmid pMALcHT (33, 44) was used to express LipL1, HK96A, HK96M-LipL1 fusion protein, and HK96A-LipL1 fusion protein as maltose binding protein (MBP) fusion proteins with a linker region composed of a tobacco etch virus (TEV) protease cut site followed by a six histidine affinity tag.

Protein expression and purification

Plasmids pMALcHT-LipL1, pMALcHT-HK96A, pMALcHT HK96M-LipL1, pMALcHT HK96A-LipL1, pMALcHT HK96A-LipL1 d15, and pMALcHT HK96A-LipL1 d9 were transformed into BL21-Star (DE3) cells (Invitrogen) and co-transformed with the pRIL plasmid isolated from BL21- CodonPlus-RIL cells (Agilent) and plasmid pRK586 encoding the Tobacco Etch Virus (TEV) protease (45), as previously described (33, 42). These cells produce the protein of interest fused to an amino-terminal six histidine-tag (the MBP tag is cleaved *in vivo* by TEV protease). Transformed cells were grown in 500mL of Terrific Broth (TB) at 250rpm, 37^{o}C until OD (600nm) = 3.0. The expression of recombinant proteins was induced by the addition of 0.4mM IPTG and cultures were incubated for 10 hours at 20^{o}C. Proteins were harvested by pelleting cultures at 4200rpm for 20 minutes. Cell pellets were re-suspended in approximately 50mL of buffer containing 20mM HEPES, 300mM NaCl, 20mM imidazole, pH 7.5 and supplemented with EDTA free protease inhibitor cocktail, (Complete Protease Mini; Roche Diagnostics Corp.). Re-suspended cells were cooled on ice and lysed via

sonication at 33% amplitude, a pulse of 0.5s on, 0.5s off, in three 1-minute iterations, with one minute of cooling between sonication. Lysed cells were centrifuged at 19000rpm for 25 minutes. The supernatant was then subjected to metal chelate chromatography (HisTrap HP 5mL). Captured protein was gradient eluted with 1M imidazole pH 8.0 into 5mL fractions. Fraction samples were analyzed via SDS-PAGE. Fractions containing the protein of interest were consolidated and subjected to desalting/buffer exchange (20mM HEPES, 50mM NaCl, pH 7.5 for HK96A and LipL1 or 50mM MES, 50mM NaCl, pH 6.0 for H-LipL1 fusion) with 2x HiPrep 26/10 columns with the flow through passing directly onto ion exchange columns (HiTrap SP FF 5mL column for LipL1 and H-LipL1 fusion: HiTrap Q HP 5mL column for HK96A). Proteins were gradient eluted from ion exchange columns with 20mM HEPES, 1M NaCl, pH 7.5 for HK96A and LipL1 or 50mM MES, 1M NaCl, pH 6.0 for H-LipL1 fusion and collected in 5mL fractions. Fraction samples were analyzed via SDS-PAGE. Fractions containing the protein of interest were consolidated and subjected to gel filtration/size exclusion chromatography on a HiPrep 26/60 Sephacryl S-100 high resolution column. Proteins were collected in 5 mL fractions that were analyzed via SDS-PAGE. Fractions containing the protein of interest were consolidated and concentrated using Amicon Ultra centrifugal filters, 10kD MWCO and 30kD MWCO for HK96A and LipL1, respectively. Purity was confirmed by SDS-PAGE using Coomassie staining. Stock protein quantification was performed using a Nanodrop ND-2000 spectrophotometer at 280nm absorbance. The absorbance values along with the predicted extinction coefficient obtained through the ExPASy protparam tool (http://web.expasy.org/protparam) were

used to calculate the protein concentration. Concentrated protein stocks were used immediately or stored at -80^{o}C. All purification techniques were conducted at 4^{o}C using an AKTA FPLC system. All columns used were manufactured by GE Healthcare Life Sciences.

Crystallization

Purified LipL1 and HK96A were thawed on ice and spun at 13000rpm for 15 minutes at 4^{o}C in a tabletop centrifuge to pellet any aggregates, the supernatant was transferred to a clean Eppendorf tube after centrifugation. Purified, concentrated LipL1, HK96A, ATP and R-Lipoic acid were combined into a master mix with final concentrations of 100µM, 130µM, 1mM, and 130µM, respectively.

Initial crystal screening conditions were performed using a 96-well 3 sitting drop Intelli-Plate (Art Robbins Instruments). Crystals were identified from a screen set up with 200nL of the above master mix and 200nL reservoir using a Mosquito crystallization robot (TTP Labtech). The Hampton Crystal Screen, MORPHEUS protein crystallization screen (MRC Labs), and the Wizard Classic crystal screen (Rigaku) were used in the initial screening conditions. Crystals were observed in the Hampton crystal screen, conditions 6, 12, and 46. Crystal optimization was attempted around these conditions using a 24-well 4 sitting drop Intelli-Plate with reservoir containing 500µL of mother liquor. Sitting drops contained 1µL of the above master mix and 1µL of reservoir solution. All trays were covered and placed in 20^{o}C to equilibrate. See appendix for optimization conditions. Crystal optimization was unsuccessful. Initial screen crystals were mounted

in a 0.1mm nylon cryoloop (Hampton Research) and flash frozen directly in liquid nitrogen before shipping to the Stanford Synchrotron Radiation Lightsource (SSRL) for data collection.

Purified HK96A-LipL1 fusion protein was thawed on ice and spun at 13000rpm for 15 minutes at 4^{o}C in a tabletop centrifuge to pellet any aggregates and the supernatant was transferred to a clean Eppendorf tube after centrifugation. Purified, concentrated HK96A-LipL1, ATP and R-Lipoic acid were combined into a master mix with final concentrations of 60µM (3.2 mg/mL), 1mM, and 100µM, respectively. Initial screening conditions were carried out as described above using the following screens: Hampton Crystal Screen, MORPHEUS protein crystallization screen (MRC Labs), Wizard Classic I and II crystal screens (Rigaku), PEGs Suite (Qiagen), Classics Suite (Qiagen). No crystals were observed in any of these conditions. Optimization was not attempted.

Isothermal Titration Calorimetry

HK96A and LipL1 were thawed on ice and dialyzed overnight at 4^{o}C in 1L of 50mM TRIS-HCl pH 7.4, 150mM NaCl using 3,500 molecular weight cut off Slide-A-Lyzer dialysis cassettes (Pierce). ITC experiments were carried out using a MicroCal VP-ITC calorimeter. A titrant containing 20-fold molar excess of HK96A was titrated into a 1.4mL sample of 2µM LipL1 at 25^{o}C. Both titrant and sample cell solutions contained 100µM ATP, 100µM $MgCl_2$, and 100µM R-lipoic acid. For one experiment, 5mM TCEP was added in addition to the above small molecules. A single 2µL injection followed by twenty-nine 5µL injections was used for each experiment. The baseline was corrected manually and the corrected data were fit to a single-site binding model using Origin

software. Experiments not containing TCEP were carried out in triplicate and the experiment containing 5mM TCEP was performed only once due to limited quantities of HK96A.

Surface Plasmon Resonance

SPR data was collected on a Biacore 3000 instrument. All protein solutions were spun at 13000rpm for 15 minutes at 4^{o}C in a tabletop centrifuge to remove any aggregates prior to data collection. All buffers were filtered through a 0.22-micron sterile filter device and degassed prior to use. Each time a new sensor chip was docked or running buffer was replaced, the system was primed three times to flush and equilibrate all internal pumps, tubing and chambers. Purified, concentrated LipL1 or HK96A was diluted to 20-50µg/ml in 200µL of 10mM sodium acetate buffer at pH 6.5, 6.0, 5.5, 5.0, 4.5, 4.0 and pH scouting for optimal pre-concentration conditions on sensor chips CM5 and CM3 was performed. This procedure identifies the pH conditions that maximize protein accumulation on the sensor chip surface due to electrostatic interactions between the protein to be bound (ligand) and the carboxymethylated dextran (pK_a = 3.5) on the sensor chip surface. Inspection of the sensorgram during pre-concentration will indicate what pH is ideal for covalent immobilization, but also at what pH, if any, your protein may be denaturing and aggregating on the sensor surface. This is indicated by a persistent response on the sensor surface after the pre-concentration step has completed. Sodium acetate pH 5 was determined to be the best pre-concentration buffer for immobilization of HK96A, while sodium acetate pH 6 was the best pre-concentration buffer for LipL1. During pre-concentration at pH 5.5 or below,

LipL1 became “stuck” to the sensor chip surface and was unable to be removed even after harsh treatment with 50mM NaOH and 0.5% SDS. HK96A showed no indications of denaturation during pre-concentration.

HK96A or LipL1 were immobilized to the surface of a particular flow cell via amine coupling with 0.4M EDC/0.1M NHS using the Biacore surface preparation wizard. Coupling reactions were quenched with 1M ethanolamine pH 8.5. Chips were allowed to equilibrate for at least 2 hours in running buffer at a flow rate of 5µL/min following the coupling procedure. The reference flow cell was subjected to the same EDC/NHS coupling chemistry and ethanolamine quenching as the experimental flow cell, however no ligand was ever bound to the surface of the reference flow cell. The analyte was diluted in running buffer and a series of 2 fold dilutions were performed. Binding experiments were performed at a flow rate of 30µL/min, analyte injections were carried out using the kinetic injection (KINJECT) command in order to minimize analyte dispersion within the flow chambers prior to reaching the flow cell, an association time of 60 seconds (minimum), and a dissociation time of 120 seconds (minimum). Regeneration conditions could not be experimentally determined, therefore, after the dissociation step in each injection cycle, the flow rate was increased to 50µL/min for 10 minutes prior to the next injection. This long wait time was added in order to allow for continued dissociation of the analyte ligand complex. Every binding experiment began with three blank injections of running buffer, that served to “warm-up” the instrument as well as provide a valuable second reference during data analysis. A single running buffer blank injection was also included in between the analyte concentration series

injections.

Data was analyzed using Scrubber (BioLogic) software. To correct for non-specific binding and baseline drifts, a double referencing method was applied using the reference flow cell as well as interspersed blank injections.

Results

Protein Purification

Typical yield from a 2 x 500mL Terrific Broth preparation of HK96A is 250µL at 2.0 mg/mL. Typical yield from a 2 x 500mL Terrific Broth preparation of LipL1 is 1mL at 8 mg/mL. Both proteins appear to be greater than 90% pure (figure 5c). Both HK96A and LipL1 elute well past the void volume (90mL) of the 26/60 Sephacryl S100 column (figure 5a and 5b), indicative of a protein that has retained its native conformation and has not aggregated to form a large particle.

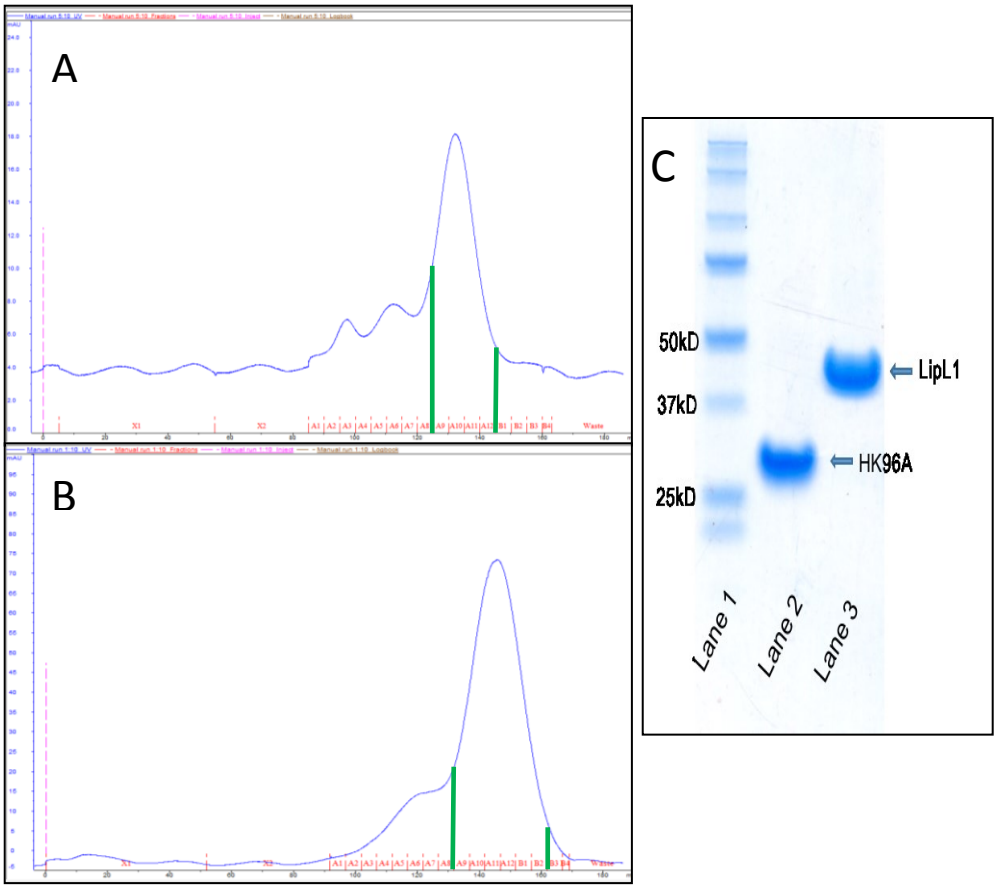

Figure 5 – HK96A and LipL1 protein purification. (A) Typical gel filtration elution profile for HK96A, in this purification fractions A9-A12 (green lines) were pooled and concentrated. HK96A begins to elute around 120mL. (B) Typical gel filtration elution profile for LipL1, fractions A9-B2 were pooled and concentrated. LipL1 begins to elute around 130mL. (C) SDS-PAGE gel of purified, concentrated HK96A and LipL1. Lane 1- ladder, Lane 2- Purified HK96A, Lane 3- Purified LipL1.

Typical yields from a 4L LB broth preparation of HK96A-LipL1 full length fusion protein was 1.1mL at 7.4 mg/mL. Typical yields from a 2L LB broth preparation of HK96A-LipL1 d15 fusion protein was 1.5mL at 2.1 mg/mL. The H-protein (19.2kD) has a theoretical isoelectric point of 4.74, while LipL1 (41.1kD) has a theoretical isoelectric point of 8.51. I assumed that the H-protein and LipL1 in the fusion protein construct would behave as independent globular proteins. After metal chelate chromatography using the HisTrap column, I chose to take advantage of the larger positively charged LipL1 for the ion exchange purification step. I found that by using 50mM MES at pH 6.0, I

could increase the purity of the fusion protein during elution from the SP column, when compared to 20mM HEPES at pH 7.5 which was the buffer used during the ion exchange step for each of the individual proteins. The HK96A-LipL1 full length and HK96A-LipL1 d15 fusion proteins can be seen below in figure 6. Neither of these protein constructs were subjected to size exclusion chromatography.

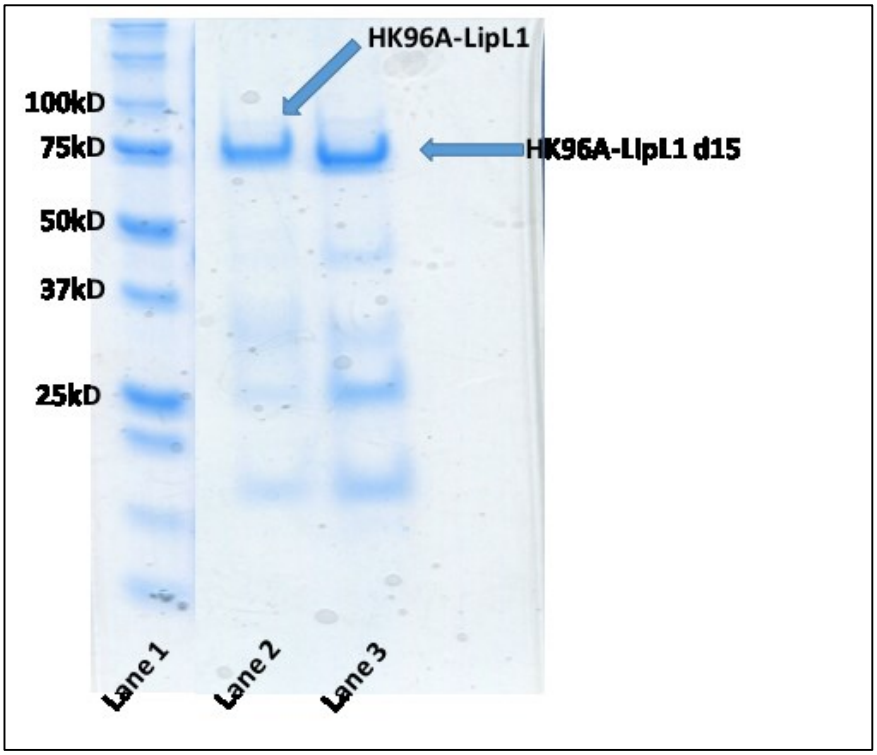

Figure 6 – Fusion protein purification. SDS-PAGE gel of purified HK96A-LipL1 fusion protein. Lane 1 is the ladder. Lane 2 is the full length HK96A-LipL1 fusion protein. Lane 3 is the HK96A-LipL1 d15 fusion protein. The predicted size of the HK96A-LipL1 fusion protein is 61,700kD while the HK96A-LipL1 d15 fusion protein is 60300kD. Lanes represent proteins after two steps of purification: metal chelate chromatography with a HisTrap column followed by SP cation exchange.

Crystallization

Four LipL1/lipoyl-AMP/HK96A complex crystals were sent to SSRL, but did not produce a diffraction pattern of significant quality and therefore could not be used for

further structural studies. On a positive note, the diffraction pattern was not that which is characteristic of a salt crystal. Upon return of the crystals from the SSRL, they were washed and subjected to SDS-PAGE in an attempt to visualize which protein(s) actually crystallized. Protein bands were not visible in the SDS-PAGE lanes following two days of staining.

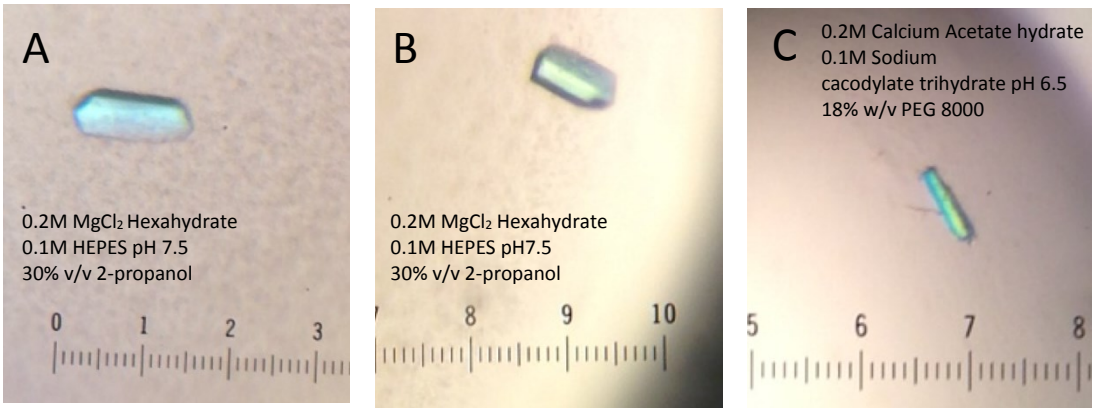

Figure 7. LipL1-HK96A protein complex crystals. (A) One of two presumed protein complex crystals grown in Hampton Research Crystal Screen (HR), condition #12. (B) The second of two presumed protein complex crystals grown in HR, condition #12. (C) Sole crystal grown in HR, condition #46. (Not pictured crystal grown in HR, condition #6 – 0.2M $MgCl_2$ hexahydrate, 0.1M TRIS-HCl pH 8.5, 30% w/v PEG 4000).

Isothermal Titration Calorimetry

Prior to adding 40µM HK96A into the injection syringe and 2µM LipL1 into the sample cell, both proteins were incubated with 100µM ATP, 100µM $MgCl_2$, and 100µM R-lipoic acid for 10 minutes. The small molecules were added to LipL1 in order to allow the formation of the lipoyl-AMP conjugate. The small molecules were added to HK96A in order to minimize the heat of dilution during the titration.

The average dissociation constant for the HK96A with LipL1/lipoyl-AMP interaction under non-reducing conditions (figure 8) was determined to be 0.097µM.

The dissociation constant for this interaction under reducing reductions (figure 9) is presented here as 4.8µM. The experiment under reducing conditions was only performed once due to limited amounts of purified HK96A. Table 8 (appendix) summarizes the data collected from the successful ITC.

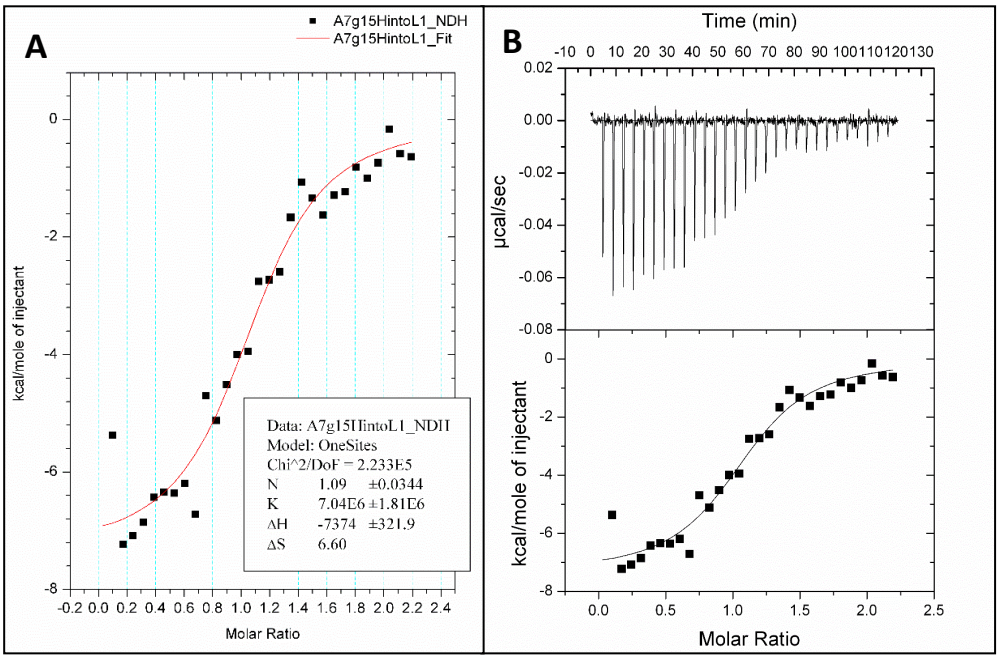

Figure 8 – ITC binding data – non-reducing conditions. (A) The binding isotherm (red) is fit to the integrated peaks (B - top panel) using a 1:1 binding model. The K_D for this experiment is 0.142µM. (B) Top panel – Each peak represents the heat released, due to binding, for each injection of HK96A into LipL1. As LipL1 becomes more saturated with each subsequent injection of HK96A, less binding and therefore less heat of binding can be measured until the only the heat of dilution is measured. (B) Bottom panel – The binding isotherms created by plotting the integrated heat peaks against the molar ratio of LipL1.

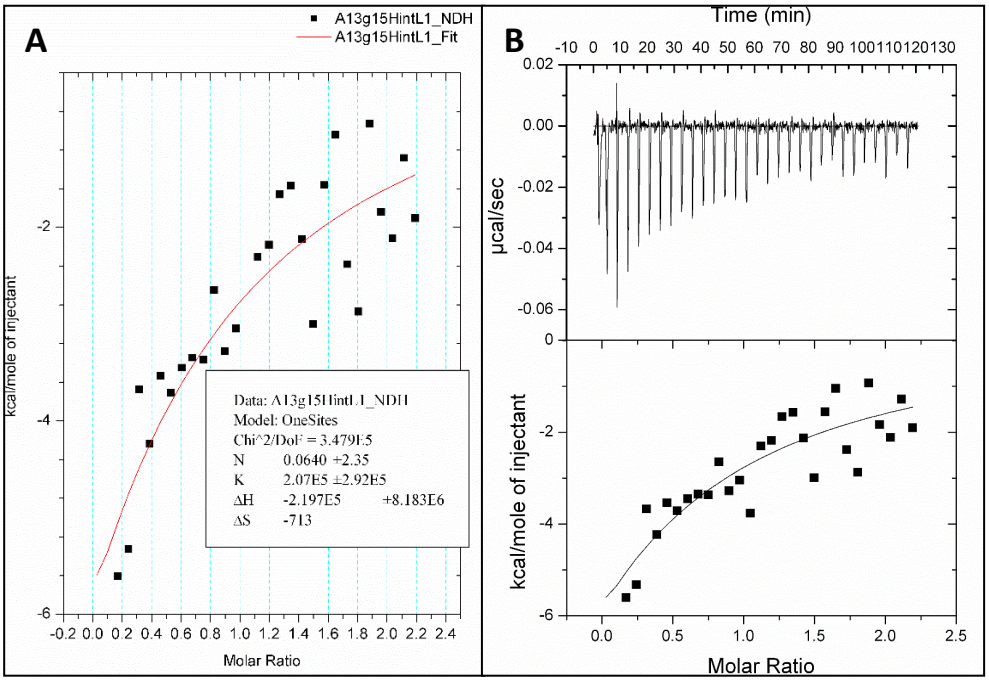

Figure 9 – ITC binding data – reducing conditions. (A) The binding isotherm (red) is fit to the integrated peaks (B - top panel) using a 1:1 binding model. The K_D for this experiment is 4.8µM.

Surface Plasmon Resonance

Numerous attempts to measure the binding affinity of the H-protein and LipL1/lipoyl-AMP were made using various buffers, at various concentrations, with additves such as BSA and soluble dextran to reduce non-specific binding and increase the signal to noise ratio. Table 7 summarizes the experimental conditions and observations from the various SPR experiments that I conducted. I initially started the SPR binding experiments using a CM5 sensor chip which has a very high density of carboxymethylated dextran. Due to the very high level of non-specific binding that was observed when flowing LipL1 or HK96A as the analyte on the CM5 chip, I abandoned the CM5 chip for a CM3 sensor chip, which has shorter dextran polymers and significantly less carboxymethylated coupling sites. The sensorgram in figure 10 was generated using

a CM3 chip with 2946 response units (RU) of LipL1 bound to chip surface. A 7mg/mL LipL1 sample was diluted in 200µL of 10mM sodium acetate buffer pH 6 to a final concentration of 35µg/mL. Flow cell 1 on the CM3 chip was activated with EDC/NHS using the Biacore surface preparation wizard. The 35µg/mL LipL1 sample was then allowed to flow into the activated flow cell 1 at 5µL/min for 1 minute in order to accomplish covalent coupling of LipL1 to the surface of the sensor chip. After 1 minute the coupling reaction was immediately quenched by the the flow of 1M ethanolamine pH 8.5 for 7 minutes. The activation, coupling, and quenching was automated and performed in immediate succession by the Biacore surface preparation wizard. I allowed the activated chip to equilibrate in the running buffer (25mM K-Na PO_4 pH 7.5, 65mM NaCl, 3mM EDTA, 0.005% (v/v) tween 20) for 4 hours before beginning binding studies. A 153µM HK96A solution was diluted to a final concentration of 5µM HK96A in running buffer with 1mM ATP and 100µM R-lipoic acid. Four, 2-fold serial dilutions of this sample were made yielding final concentrations of HK96A at 5µM, 2.5µM, 1.25µM 625nM, and 312nM.

The binding experiments were carried out at 30µL/min, with an association time of 150 seconds, dissociation time of 180 seconds, and 2 separate 60 second quick injections of 1M NaCl per cycle in an attempt to dissociate any bound H-protein (regeneration). Three “blank” running buffer injections cycles were followed by a conjugation formation injection cycle consisting of just 1mM ATP and 100µM R-lipoic acid. This conjugation formation injection cycle was followed by another blank running buffer injection and finally the concentration series injections beginning with the 5µM

HK96A concentration and proceeding to the lower concentrations. For this experiment flow cell 4 was used a subtractive reference cell and the average of the running buffer blank injections were used to double reference the sensorgram. Flow cell 4 was unmodified by any coupling chemistry. The 5µM HK96A concentration injection data was inconsistent with the other concentration sensorgram curves and was removed prior to curve fitting. The association and dissociation of the analyte HK96A to bound LipL1/lipoyl-AMP can be seen below in figure 10. Binding data from this SPR experiment with LipL1 bound and HK96A under flow, yield a dissociation constant of 0.396µM under non-reducing conditions.

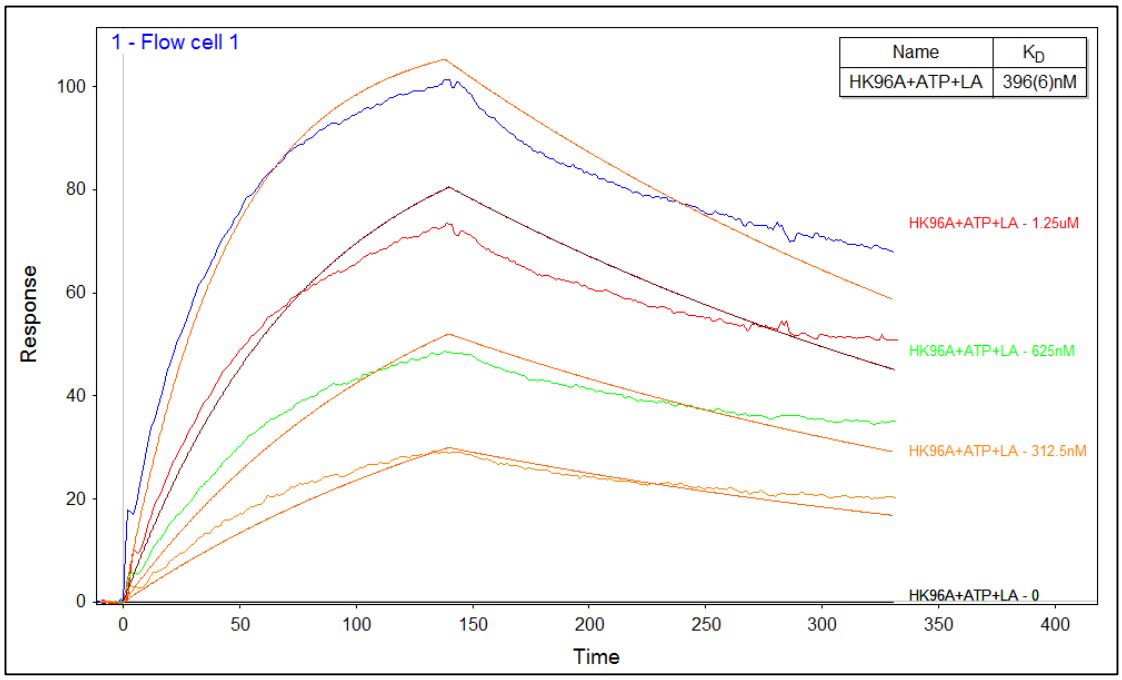

Figure 10 – SPR binding data – non-reducing conditions. His_6-LipL1 was immobilized on a CM3 chip and His_6-HK96A was injected at four 2-fold serial dilutions (2.5µM-312.5nM). The blue curve is the HK96A 2.5µM concentration injection. The sensorgram plots response units on the Y-axis vs. time on the X-axis. Straight lines over the raw sensorgram curves indicate the best fit model used by Scrubber (Biologic) data processing software to derive an equilibrium dissociation constant of 0.396µM for this interaction.

Discussion

By increasing the length of the sonication to three 1-minute iterations and by

adding 20mM imidazole to the lysis/running buffer during lysis and initial His-trap purifications, I was able to increase the yield and purity of *Pf*HK96A. This is important for future work as HK96A was the limiting reagent in all of these experiments.

It is also worth noting that the size of the *E. coli* pellet during expression of HK96A was significantly reduced as compared to the size of the *E. coli* pellet during expression of Lipl1. This casual observation could indicate that the overexpression of *Pf* HK96A is toxic to *E. coli*, possibly due to competitive binding of the *E. coli* H-protein to LplA.

Although PfHK96A is roughly half the size of LipL1 it starts to elute from the S100 gel filtration column about 10mL prior to LipL1. Typically, larger proteins tend to elute first, with smaller proteins eluting after. I performed one of the many HK96A gel purifications under reducing conditions to see if the early HK96A elution was due to dimerization through a disulfide bond. The reducing conditions had no effect on the gel filtration elution profile of HK96A, suggesting that HK96A is not a disulfide-linked dimer and therefore does not explain the early elution of HK96A. It may be that HK96A exists as a non-covalent dimer or has an unusual non-globular shape, resulting in a large hydrodynamic radius. It is worth noting that the *Pf* H-protein has an extended 40 amino acid tail not found in prokaryotic H-protein sequences and this region could be responsible for the unexpected elution profile from the gel filtration column.

The fusion protein constructs were not subjected to size exclusion chromatography prior to attempting crystallization. Getting a cleaner fusion protein, via gel filtration, prior to setting up crystal conditions could increase the chances of

producing ternary complex crystals that produce diffraction patterns at high enough resolution that lead to structural determination.

I moved away from ITC as a technique for determining the binding affinities for the protein-protein interaction due to that fact that each experiment consumed a large quantity of the purified HK96A protein used as the titrant. Typical yields for a 5-day long expression and purification from the gel filtration column were 250µL at 2mg/mL. A 2mg/mL concentration of HK96A is roughly 120µM. For the single experiment shown in Figure 8, 350µL of 40µM HK96A was used. I turned to SPR as a second method to determine the binding affinities of the proteins. Due to the highly sensitive nature of the technique very small quantities of proteins are needed. In theory, this should facilitate studying this interaction since HK96A is poor overexpressing protein and it is difficult to obtain large amounts.

SPR was not without its challenges. One of the major challenges of capturing the binding response was overcoming the response due to non-specific binding (NSB) of the analyte to the sensor chip surface. Theoretically, you can run SPR experiments with either binding partner bound to the chip surface. I tried multiple experiments with HK96A bound to the chip surface and flowing LipL1 as the analyte. I could not find conditions to overcome the LipL1 non-specific binding response. I settled on the amine coupling of LipL1 to the chip with HK96A as the analyte, as early experiments showed that HK96A had significantly less NSB. I was finally able to get a characteristic binding sensorgram after switching to a less carboxymethylated CM3 sensor chip. Results from the dilution series SPR experiment described above suggest a dissociation constant of

396nM under non reducing conditions, which is not far from the 97nM dissociation constant calculated under non-reducing conditions using ITC.

The binding data from the ITC experiments suggest that HK96A does indeed have an increased affinity for LipL1/lipoyl-AMP under non-reducing conditions as compared to reducing conditions. It remains to be seen whether the SPR experiment will yield reproducible results and a similar SPR experiment has yet to be conducted in the presence of a strong reducing agent, in order to compare the SPR dissociation constant under reducing conditions to that calculated by ITC. In the absence of structural data, it is impossible to explain why LipL1 preferentially lipoylates the H-protein under non-reducing conditions vs. reducing conditions. In order to draw a complete picture of the mechanism of this pathway it is necessary to solve the crystal structures of the LipL1/lipoyl-AMP/H-protein complex as well as LipL1 in complex with dihydrolipoyl-AMP or its structural analogue 6,8 dichlorooctanoate to corroborate what we are seeing with the binding data of these two proteins.

Further inquiries into the actual role of the H-protein are also needed to understand the H-protein's role after it is lipoylated. The P and T proteins of the GCS are absent in *Plasmodium falciparum*; therefore, the H-protein cannot perform its canonical role in glycine metabolism. It may be that the *Pf* H-protein has a function similar to that recently elucidated in *Trichomonas vaginalis* (46). In *T. vaginalis*, the P and T proteins are absent, with the H and L proteins being found in the hydrogenosome. It was shown that the H and L proteins work to deliver electrons to osmotically inducible protein, OsmC, which in turn reductively detoxifies harmful peroxides which are formed during

the interaction between the host's immune response and *T.vaginalis* parasites (46).

Appendix

Primers used for site directed mutagenesis, lysine to alanine mutation at position 96 of the *Plasmodium falciparum* H-protein.

Forward:
5’ – GATTGTATAGCGACAATTGAAAGTGTCgcgAGTGTAGGAGATGTATATACTCCTGT-3’

Reverse:
5’ – ACAGGAGTATATACATCTCCTACACTcgcGACACTTTCAATTGTCGCTATACAATC-3’

Primers used for creating the adaptamer in order to change methionine at position 96 in the HK96M-LipL1 fusion protein to alanine, yielding the HK96A-LipL1 fusion protein

Forward:
5’ – Phos-CGAAAGTGTCgcgAGTGTAGGAGACGT – 3’

Reverse:
5’ – Phos-CTCCTACACTcgcGACACTTTCGAT – 3’

Primers used for sequencing the pMALcHT plasmid.

Forward:
5’ – GCCCTGAAAGACGCGCAGAC – 3’

Reverse:
5’ – CGCCAGGGTTTTCCCAGTCACGAC – 3’

GGAATTGTGAGCGGATAACAATTCCTAGGAGGAGGTTGGATCCATGGAATTCATTAAAATCGA
AGATGGCAATCTGAACAACCGCAAAGATATGACCAATGTGAAATGCAAAATTGGCATCAGCAA
TTACGGCACCCATAAACTGGGTGAAATTGTTTATGTTGATGTGGCCCATAACATCAACGACCAT
GTTAAAAAAGGTGATTGCATTGCAACGATCGAAAGCGTTATGAGCGTTGGTGACGTCTATACA
CCGGTTAGCGGCAAAATTATCAATATCAACAACAAAATCATCGATAACGTGAACCTGATGAAC
GAACAGAGCGAAATTGATGGTTGGATTATGGAACTGGAAACCAACCAGATCAACGAAAAAGA
AATTATGAACATCAGCGAATATGAAAAAATGTGCGAGGAAGAAGAACAGAACGAAGAGAAA
AAAATCCAGCAGAACGAGATCAATTGCATGGAAGAAAAAAACAAAAACAAAATCTTTGATATT
AATGACATGAAAAACATCGAAAACAAAGGCCAGGGTGGTAAAACTAGTAGCGGTACCTCTGG
GCCCAGCGGGCCCTCTGGTACCAGCGCTAGCAATGGTCCGCTGGTTCTGGTTAGCAATAATCA
GAACATTCACTTTAACCTGAGCCTGGAAAACTTTCTGCTGAACAACTATAACGACCTGCTGAAA
TATCTGAACATTAACACCATCGAGAAATTCAACGAACCGATTCTGTTTCTGTGGCGTAATAATC
GCAGCATTATTATCGGCAAAAACCAGAACATTTGGAGCGAATGTAACCTGAAAAACATTAAAG
AAGATGGCGTTCTGGTTGCACGTCGTTTTACCGGTGGTGGTGCAGTTTATCACGATCTGGGTA
ATGTTTGTTTTACCTTCCTGAACAACAACATCAATACCAGCAGCAACTTTCTGATCATTCTGAAC
ACCCTGAAAAATCACTTCAACATCGAAGCAAAAACCCAGGGTCGTAATGATATTACCGTTAAC
GATCAGAAATGTAGCGGTAGCGCATTCAAAAAAATCAAAGATGTGTTTCTGCATCACGGCACC
ATTCTGATTAATCTGGAAAAAAACATCCTGAACAAATATCTGACACCGGACAAAATCAAATATA
TCAAACATGGTGTGAGCAGCGTTAATGCCCGTACCATTAATCTGAGCGAAATCAACAATAACA
TCACGTGCGAGAATTTATGCATTGCCCTGATCAAAGAATTTACCAAATTCTACGAGCAGAACTA
CAACACCAACATTATTCCGAACGACATCACTGTACATTATATCGATCAGAATAACAACATTACC
AAAAATCCGGAATTTCTGAAATATTACAATCTGCTGAAAGACTGGGATTGGTGCTATGGTAAA
ACCCCGAAATTTCAGAACCATATCTGGAAACAGTTTACCTTCGGTAAACTGGAACTGTTTTTTA
ACGTGAGCAACGGCTTCATTAAAGACGGCAACATTTTTAGCGATTGCCTGGATATTAACCTGAT
CGACCATCTGAAAAGCATCTTCAACAACGATATCAAATACAGCAAAGAGGATATCAGCATCTTT
TTCAAAAAACTGAACGTCGAGAACAAAAACTATCTGGATGAAGTTCGTAGCTGGATTCTGCAA
GAGCTCTAGAGGAGGTCACCATCACCATCACCATTGAAAGCTTCTCGAGCTTAAG

Figure 11 – HK96M-LipL1 DNA sequence. Synthetic DNA sequence purchased from GeneArt which codes for the HK96M-LipL1 fusion protein. Red text represents the H-protein sequence, green text is the 17 amino acid linker, purple text is the LipL1 sequence. The highlighted bases represent the methionine that was mutated to alanine for this thesis work. The first and last underlined bases represent restriction enzyme (RE) cut sites EcoRI and HindIII respectively. The underlined bases on the same line with the highlighted methionine bases are the PvuI and AatII RE cut sites, which were used to insert the adaptamer coding for the alanine mutation. Underlined bases in the 17AA linker are the SpeI, KpnI, KpnI, and NheI RE cut sites which were used to adjust the length of the linker between the two proteins.

MEFIKIEDGN LNNRKDMTNV KCKIGISNYG THKLGEIVYV DVAHNINDHV KKGDCIATIE
SVMSVGDVYT PVSGKIININ NKIIDNVNLM NEQSEIDGWI MELETNQINE KEIMNISEYE
KMCEEEEQNE EKKIQQNEIN CMEEKNKNKI FDINDMKNIE NKGQGGKTSS GTSGPSGPSG
TSASNGPLVL VSNNQNIHFN LSLENFLLNN YNDLLKYLNI NTIEKFNEPI LFLWRNNRSI
IIGKNQNIWS ECNLKNIKED GVLVARRFTG GGAVYHDLGN VCFTFLNNNI NTSSNFLIIL
NTLKNHFNIE AKTQGRNDIT VNDQKCSGSA FKKIKDVFLH HGTILINLEK NILNKYLTPD
KIKYIKHGVS SVNARTINLS EINNNITCEN LCIALIKEFT KFYEQNYNTN IIPNDITVHY
IDQNNNITKN PEFLKYYNLL KDWDWCYGKT PKFQNHIWKQ FTFGKLELFF NVSNGFIKDG
NIFSDCLDIN LIDHLKSIFN NDIKYSKEDI SIFFKKLNVE NKNYLDEVRS WILQEL

Figure 12 – HK96M-LipL1 amino acid sequence. Colored and highlighted text corresponds to figure 12.

	1	2	3	4	5	6	
A							20% 2-propanol (v/v)
B							25% 2-propanol (v/v)
C							30% 2-propanol (v/v)
D							35% 2-propanol (v/v)
	0.1M Na Cacodylate pH 6.4	0.1M Na Cacodylate pH 6.8	0.1M HEPES pH 7.4	0.1M HEPES pH 7.6	0.1M TRIS-HCl pH 8.0	0.1M TRIS-HCl pH 8.2	

Table 2 – Crystal tray optimization conditions #1. Optimization tray setup for attempt at co-crystallization of HK96A, LipL1, Lipoyl-AMP complex. No crystals were observed in these conditions.

	1	2	3	4	5	6	
A							0.2 M HEPES pH 7.5 0.4 M MgCl
B							0.15 M HEPES pH 7.5 0.3 M MgCl
C							0.125 M HEPES pH 7.5 0.25 M MgCl
D							0.1 M HEPES pH 7.5 0.2 M MgCl
	5% 2-propanol (v/v)	10% 2-propanol (v/v)	15% 2-propanol (v/v)	20% 2-propanol (v/v)	25% 2-propanol (v/v)	30% 2-propanol (v/v)	

Table 3 – Crystal tray optimization conditions #2. Optimization tray setup for attempt at co-crystallization of HK96A, LipL1, Lipoyl-AMP complex. No crystals were observed in these conditions.

	1	2	3	4	5	6	
A							0.2 M Na Cacodylate pH 6.5 0.4 M Ca Acetate
B							0.15M Na Cacodylate pH 6.5 0.3 M Ca Acetate
C							0.1 M Na Cacodylate pH 6.5 0.2 M Ca Acetate
D							0.05 M Na Cacodylate pH 6.5 0.1 M Ca Acetate
	30% PEG 8000	25% PEG 8000	20% PEG 8000	18% PEG 8000	15% PEG 8000	12% PEG 8000	

Table 4 – Crystal tray optimization conditions #3. Optimization tray setup for attempt at co-crystallization of HK96A, LipL1, Lipoyl-AMP complex. No crystals were observed in these conditions.

	1	2	3	4	5	6	
A							30% PEG 4000 (w/v)
B							20% PEG 4000 (w/v)
C							15% PEG 4000 (w/v)
D							10% PEG 4000 (w/v)
	0.1M TRIS-HCl pH 8.0 0.2M MgCl	0.1M TRIS-HCl pH 8.2 0.2M MgCl	0.1M TRIS-HCl pH 8.4 0.2M MgCl	0.1M TRIS-HCl pH 8.6 0.2M MgCl	0.1M TRIS-HCl pH 8.8 0.2M MgCl	0.1M CAPS pH 9.0 0.2M MgCl	

Table 5 – Crystal tray optimization conditions #4. Optimization tray setup for attempt at co-crystallization of HK96A, LipL1, Lipoyl-AMP complex. No crystals were observed in these conditions.

	1	2	3	4	5	6	
A							30% PEG 4000 (w/v)
B							20% PEG 4000 (w/v)
C							15% PEG 4000 (w/v)
D							10% PEG 4000 (w/v)
	0.1M Na Cacodylate pH 6.4 0.2M MgCl	0.1M Na Cacodylate pH 6.8 0.2M MgCl	0.1M HEPES pH 7.0 0.2M MgCl	0.1M HEPES pH 7.2 0.2M MgCl	0.1M HEPES pH 7.4 0.2M MgCl	0.1M HEPES pH 7.6 0.2M MgCl	

Table 6 – Crystal tray optimization conditions #5. Optimization tray setup for attempt at co-crystallization of HK96A, LipL1, Lipoyl-AMP complex. No crystals were observed in these conditions.

Chip Type	Buffer	Coupling	Ligand	Analyte	Observations	Results
Ni-NTA	10mM HEPES 150mM NaCl 3mM EDTA 0.005% p20	Capture	6x His-LipL1	GST-HK96M	Drifting Baseline NSB	No kinetic data Affinity based on equilibrium concentration K_D- 310nM from first pass experiment Ni-NTA chip costly, highly reusable, no need for regen
CM5	10mM HEPES 150mM NaCl 3mM EDTA 0.005% p20	Amine Coupling	6x His-LipL1	6xHis-HK96A	Non specific binding	High NSB with this chip. Could be due to amine coupling LipL1 @ pH 5 With 100-300RU of LipL1 bound insignificant binding response
CM5	10mM HEPES 150mM NaCl 3mM EDTA 0.005% p20	Amine Coupling	6xHis-HK96A	6xHis-LipL1	Non specific binding	Inconclusive Too much NSB. LipL1 seems to be very sticky.
CM3	10mM HEPES 150mM NaCl 3mM EDTA 0.005% p20	Amine coupling	6x His-HK96A	6xHis-LipL1	Non-specific binding	Less NSB than with CM5 chip. CM3 chip has shorter dextran. LipL1 has high NSB. Could not be overcome with soluble dextran or BSA
CM3	30mM PO_4 65mM NaCl 3mM EDTA 0.005% p20	Amine coupling	6x His-LipL1	6xHis-HK96A	Decent sensorgrams	At 5µM analyte plateaus at low RU At 2.5µM -600nM analyte conc. yields characteristic binding sensorgram Coupled 2900RU of LipL1 to surface-may be necessary in order to get decent signal due to random and cross coupling to dextran matrix

Table 7 – SPR experimental notes.

ITC Experiment	Buffer	Cofactors	Titrant	Sample cell	TCEP	N	K_D	Average K_D
1	50mM TRIS-HCl 150mM NaCl pH 7.4	100µM ATP 100µM $MgCl_2$ 100µM R-LA	40µM HK96A	2µM LipL1	NO	1.1	0.142µM	-
2	50mM TRIS-HCl 150mM NaCl pH 7.4	100µM ATP 100µM $MgCl_2$ 100µM R-LA	40µM HK96A	2µM LipL1	NO	0.91	0.071µM	-
3	50mM TRIS-HCl 150mM NaCl pH 7.4	100µM ATP 100µM $MgCl_2$ 100µM R-LA	40µM HK96A	2µM LipL1	NO	0.95	0.077µM	-
								0.097µM
4	50mM TRIS-HCl 150mM NaCl pH 7.4	100µM ATP 100µM $MgCl_2$ 100µM R-LA	40µM HK96A	2µM LipL1	YES 5mM	0.06	4.83µM	-

Table 8 – ITC results.

References

1. World Health Organization (2015) World Malaria Report 2015. 2015: ISBN 978 92 4 156515 8.
2. Klein, E.Y. (2013) Antimalarial drug resistance: a review of the biology and strategies to delay emergence and spread. *International Journal of Antimicrobial Agents*, **41**, 311–317.
3. Payne, D. (1987) Spread of chloroquine resistance in Plasmodium falciparum. *Parasitology Today*, **3**, 241–246.
4. Packard, R.M. (2014) The Origins of Antimalarial-Drug Resistance. *The New England journal of medicine*, **371**, 397–399.
5. Ducati, R.G., Namanja-Magliano, H. a and Schramm, V.L. (2013) Transition-state inhibitors of purine salvage and other prospective enzyme targets in malaria. *Future medicinal chemistry*, **5**, 1341–60.
6. Roper, C., Pearce, R., Bredenkamp, B., Gumede, J., Drakeley, C., Mosha, F., et al. (2003) Antifolate antimalarial resistance in southeast Africa: A population-based analysis. *Lancet*, **361**, 1174–1181.
7. Heinberg, A. and Kirkman, L. (2015) The molecular basis of antifolate resistance in Plasmodium falciparum: Looking beyond point mutations. *Annals of the New York Academy of Sciences*, **1342**, 10–18.
8. Mita, T. (2010) Origins and spread of pfdhfr mutant alleles in Plasmodium falciparum. *Acta Tropica*, **114**, 166–170.
9. Wongsrichanalai, C., Pickard, A.L., Wernsdorfer, W.H. and Meshnick, S.R. (2002) Epidemiology of drug-resistant malaria. *Lancet Infectious Diseases*, **2**, 209–218.
10. Pinichpongse, S., Doberstyn, E.B., Cullen, J.R., Yisunsri, L., Thongsombun, Y. and Thimasarn, K. (1982) An evaluation of five regimens for the outpatient therapy of falciparum malaria in Thailand 1980-81. *Bulletin of the World Health Organization*, **60**, 907–912.
11. Cortese, J.F., Caraballo, A., Contreras, C.E. and Plowe, C. V (2002) Origin and dissemination of Plasmodium falciparum drug-resistance mutations in South America. *J Infect Dis*, **186**, 999–1006.
12. Müller, I.B. and Hyde, J.E. (2010) Antimalarial drugs: modes of action and mechanisms of parasite resistance. *Future microbiology*, **5**, 1857–1873.
13. Ashley, E. a., Dhorda, M., Fairhurst, R.M., Amaratunga, C., Lim, P., Suon, S., et al. (2014) Spread of Artemisinin Resistance in Plasmodium falciparum Malaria. *New England Journal of Medicine*, **371**, 411–423.
14. World Health Organization and Others (2006) WHO briefing on Malaria Treatment Guidelines and artemisinin monotherapies. *Geneva: WHO*, 2006.
15. Tun, K.M., Imwong, M., Lwin, K.M., Win, A.A., Hlaing, T.M., Hlaing, T., et al. (2015) Spread of artemisinin-resistant Plasmodium falciparum in Myanmar: a cross-sectional survey of the K13 molecular marker. *The Lancet Infectious Diseases*, **15**, 415–421.
16. Imwong, M., Jindakhad, T., Kunasol, C., Sutawong, K., Vejakama, P. and Dondorp,

A.M. (2015) An outbreak of artemisinin resistant falciparum malaria in Eastern Thailand. *Scientific Reports*, **5**, 17412.
17. Reed, L.J., Debusk, B.G., Gunsalus, I.C. and Hornberger, C.S. (1951) Crystalline α - Lipoic Acid: A Catalytic Agent Associated with Pyruvate Dehydrogenase Author(s): Lester J. Reed, Betty G. DeBusk, I. C. Gunsalus and Carl S. Hornberger Source: *Science*, **114**, 93–94.
18. Yi, X. and Maeda, N. (2005) Endogenous Production of Lipoic Acid Is Essential for Mouse Development. *Molecular and Cellular Biology*, **25**, 8387–8392.
19. Morris, T.W. and Reed, K.E. (1995) Lipoic acid metabolism in Escherichia coli : the lplA and lipB genes define redundant pathways for ligation of lipoyl groups to apoprotein . T W Morris , K E Reed and J E Cronan Jr Lipoic Acid Metabolism in Escherichia coli : the lplA and lipB Genes Defin. **177**, 1–10.
20. Spalding, M.D. and Prigge, S.T. (2010) Lipoic acid metabolism in microbial pathogens. *Microbiology and molecular biology reviews : MMBR*, **74**, 200–228.
21. Morris, T.W., Reed, K.E. and Cronan, J.E. (1994) Identification of the gene encoding lipoate-protein ligase A of Escherichia coli: Molecular cloning and characterization of the lplA gene and gene product. *Journal of Biological Chemistry*, **269**, 16091–16100.
22. M. Marletta, J.E.C.X.Z.J.R.M.Y.J. (2003) Assembly of the Covalent Linkage between Lipoic Acid and its Cognate Enzymes. *Chemistry & Biology*, **10**, 1293–1302.
23. Ali, S., Moir, A. and Ashton, P. (1990) Octanoylation of the lipoyl domains of the pyruvate dehydrogenase complex in a lipoyl-deficient strain of Escherichia coli. *Molecular …*, **4**, 943–950.
24. Hayden, M.A., Huang, I., Bussiere, D.E. and Ashley, G.W. (1992) The Biosynthesis of Lipoic Acid. 1992.
25. Packer, L. (1995) Acide lipoic as biologycal antioxydant Review Article. *Free Radic Biol Med*, **19**, 227–250.
26. Moini, H., Packer, L. and Saris, N.-E.L. (2002) Antioxidant and prooxidant activities of alpha-lipoic acid and dihydrolipoic acid. *Toxicology and Applied Pharmacology*, **182**, 84–90.
27. Perham, R.N. (2000) Swinging Arms and Swinging Domains in Multifunctional Enzymes: Catalytic Machines for Multistep Reactions. *Annual Reviews of Biochemistry*, **276**, 961–1004.
28. Xiao, Z. and Xu, P. (2007) Acetoin Metabolism in Bacteria. *Critical Reviews in Microbiology*, **33**, 127–140.
29. Reed, L.J. (2001) A trail of research from lipoic acid to alpha-keto acid dehydrogenase complexes. *The Journal of biological chemistry*, **276**, 38329–38336.
30. Douce, R., Bourguignon, J., Neuburger, M. and Rébeillé, F. (2001) The glycine decarboxylase system: A fascinating complex. *Trends in Plant Science*, **6**, 167–176.
31. Salcedo, E., Sims, P.F.G. and Hyde, J.E. (2005) A glycine-cleavage complex as part of the folate one-carbon metabolism of Plasmodium falciparum. *Trends in parasitology*, **21**, 406–11.
32. Bahl, A., Brunk, B., Crabtree, J., Fraunholz, M.J., Gajria, B., Grant, G.R., et al. (2003) PlasmoDB: The Plasmodium genome resource. A database integrating experimental

and computational data. *Nucleic Acids Research*, **31**, 212–215.
33. Allary, M., Lu, J.Z., Zhu, L. and Prigge, S.T. (2007) Scavenging of the cofactor lipoate is essential for the survival of the malaria parasite Plasmodium falciparum. *Molecular microbiology*, **63**, 1331–44.
34. Günther, S., Wallace, L., Patzewitz, E.-M., McMillan, P.J., Storm, J., Wrenger, C., et al. (2007) Apicoplast lipoic acid protein ligase B is not essential for Plasmodium falciparum. *PLoS pathogens*, **3**, e189.
35. Foth, B.J., Stimmler, L.M., Handman, E., Crabb, B.S., Hodder, A.N. and McFadden, G.I. (2005) The malaria parasite Plasmodium falciparum has only one pyruvate dehydrogenase complex, which is located in the apicoplast. *Molecular Microbiology*, **55**, 39–53.
36. Wrenger, C. and Müller, S. (2004) The human malaria parasite Plasmodium falciparum has distinct organelle-specific lipoylation pathways. *Molecular microbiology*, **53**, 103–13.
37. Pei, Y., Tarun, A.S., Vaughan, A.M., Herman, R.W., Soliman, J.M.B., Erickson-Wayman, A., et al. (2010) Plasmodium pyruvate dehydrogenase activity is only essential for the parasite's progression from liver infection to blood infection. *Molecular Microbiology*, **75**, 957–971.
38. Falkard, B., Kumar, T.R.S., Hecht, L.-S., Matthews, K.A., Henrich, P.P., Gulati, S., et al. (2013) A key role for lipoic acid synthesis during Plasmodium liver stage development. *Cellular Microbiology*, **15**, 1585–1604.
39. Günther, S., McMillan, P.J., Wallace, L.J.M. and Müller, S. (2005) Plasmodium falciparum possesses organelle-specific alpha-keto acid dehydrogenase complexes and lipoylation pathways. *Biochemical Society transactions*, **33**, 977–80.
40. Günther, S., Matuschewski, K. and Müller, S. (2009) Knockout studies reveal an important role of Plasmodium lipoic acid protein ligase A1 for asexual blood stage parasite survival. *PloS one*, **4**, e5510.
41. Storm, J., Müller, S. and M\uller, S. (2012) Lipoic acid metabolism of Plasmodium--a suitable drug target. *Current pharmaceutical design*, **18**, 3480–9.
42. Afanador, G. a, Matthews, K. a, Bartee, D., Gisselberg, J.E., Walters, M.S., Freel Meyers, C.L., et al. (2014) Redox-dependent lipoylation of mitochondrial proteins in Plasmodium falciparum. *Molecular microbiology*, **94**, 156–71.
43. Fujiwara, K., Maita, N., Hosaka, H., Okamura-Ikeda, K., Nakagawa, A. and Taniguchi, H. (2010) Global conformational change associated with the two-step reaction catalyzed by Escherichia coli lipoate-protein ligase A. *The Journal of biological chemistry*, **285**, 9971–80.
44. Muench, S.P., Rafferty, J.B., McLeod, R., Rice, D.W. and Prigge, S.T. (2003) Expression, purification and crystallization of the Plasmodium falciparum enoyl reductase. *Acta Crystallographica - Section D Biological Crystallography*, **59**, 1246–1248.
45. Kapust, R.B. and Waugh, D.S. (2000) Controlled intracellular processing of fusion proteins by TEV protease. *Protein expression and purification*, **19**, 312–8.
46. Nývltová, E., Smutná, T., Tachezy, J. and Hrdý, I. (2016) OsmC and incomplete glycine decarboxylase complex mediate reductive detoxification of peroxides in

hydrogenosomes of Trichomonas vaginalis. *Molecular and Biochemical Parasitology*, 2016: 10.1016/j.molbiopara.2016.01.006.

Curriculum Vitae

Ryan Eduardo Rodriguez
Born: March 6, 1983 in Fayetteville, North Carolina
Permanent Address: 33 Ana Lane, Autryville, North Carolina 28318
Contact information: ryan.rodriguez15@gmail.com

Education

Johns Hopkins University School of Public Health **2014 – 2016**
ScM, Master of Science
Molecular Microbiology and Immunology
3.77 GPA

Missouri University of Science and Technology **2011**
MS, Master of Science
Environmental Engineering
4.0 GPA

The University of North Carolina at Pembroke **2001 – 2005**
BS, Bachelor of Science
Chemistry
3.72 GPA *magna cum laude*

Awards

Johns Hopkins Tuition Fellowship **2015 – 2016**
NASA/NACME Student Scholarship **2002 – 2005**
UNCP-CRC Freshman Chemistry Award **2001 – 2002**

Research Experience

Prigge Lab – Johns Hopkins School of Public Health **2014 – 2016**
Thesis Graduate Student
Thesis Title "The mechanism of binding between the *Plasmodium falciparum* H-protein and Lipoate Ligase 1." Research activities include protein expression and purification using HPLC, protein crystallization, molecular cloning, PCR, Isothermal Titration Calorimetry, Surface Plasmon Resonance

National Institute of Environmental Health Science **2004**
Biological Science Lab Technician – Summer Intern
Activities include molecular cloning, protein expression and purification

Stanford University - Department of Civil and Environmental Engineering **2003**

Summer Research Assistant – NASA/NACME program
Activities include collection of air and water samples in and around the bay area. Sample analysis.

Professional Experience

United States Army **2006 - Present**

Commissioned Officer – Engineer Branch